Influence of Turbulence Model, Grid Resolution and Free-Stream Turbulence Intensity on the Numerical Simulation of the Flow Field around an Inclined Flat Plate

M. Raciti Castelli, P. Cioppa and E. Benini

Abstract—The flow field around a flat plate of infinite span has been investigated for several values of the angle of attack. Numerical predictions have been compared to experimental measurements, in order to examine the effect of turbulence model and grid resolution on the resultant aerodynamic forces acting on the plate. Also the influence of the free-stream turbulence intensity, at the entrance of the computational domain, has been investigated. A full campaign of simulations has been conducted for three inclination angles (9°, 15° and 30°), in order to obtain some practical guidelines to be used for the simulation of the flow field around inclined plates and discs.

Keywords—CFD, lift, drag, flat plate

I. INTRODUCTION

THIS document aims to investigate the static aerodynamic loads acting on an inclined flat plate of infinite extent, immersed in an uniform flow field, in order to determine some practical guidelines to be used for the simulation of the flow field around inclined plates and discs, which is typical of several industrial applications. Non-aerodynamic shaped bodies, such as plates, discs, circular and rectangular cylinders and V-shaped prisms are in fact used in combustors, to enhance scalar mixing and to provide a flame-stabilizing region [1]. They are also adopted in air diverters, enabling hovercraft fans to determine both vertical and horizontal thrusts [2] [3], as well as in the supporting structures of photovoltaic panels which, being flexible and fragile (and, therefore, easily damageable by winds), require to be sustained by a proper framework [4]. In recent years, several investigations have been performed to enhance the comprehension of aerodynamic phenomena connected with the air flow around inclined plates. Suh and Liu [5] numerically investigated the viscous flow past a finite flat plate attached normally to an infinite wall for Reynolds numbers up to 2800, using also the Levi-Civita method to obtain the flow solution based on the free-streamline theory.

Taira et al. [6] investigated the flow over an impulsively started low-aspect-ratio flat plate for a Reynolds number of 300.

Numerical simulations, validated by experimental measurements, were performed to study the influence of aspect ratio, angle of attack and plan-form geometry on the interaction of the leading edge and tip vortices, as well as the resulting lift and drag coefficients, registering a significant influence of the aspect ratio on the wake pattern and the force experienced by the plate.

Bakić et al. [7] performed numerical simulations of air flow around the arrays of flat plate collectors, in order to provide a basis for estimating the resultant convective heat loss.

Breuer and Jovicic [1] numerically investigated the separated flow past an inclined, nominally two-dimensional flat plate for 18° angle of attack and a Reynolds number of 20,000. A strong vortex, developing almost periodically in the vicinity of the trailing edge and whose life cycle controlled the entire flow field, was observed, as well as a clockwise recirculation region of nearly constant pressure at the leeward side of the plate.

Raciti Castelli et al. [8] investigated the flow field past a vertical flat plate of infinite extent through a comparison between the predictions of a commercial CFD code and the experimental measurements performed by Fage and Johansen [9], achieving a good agreement between measured and numerical data.

Again, Raciti Castelli et al. [10] investigated the flow field around a 30° inclined flat plate of infinite span by comparing numerical predictions and experimental measurements (from: [9]), in order to assess the potential of a commercial CFD code of determining the aerodynamic forces acting on a flat plate invested by an uniform fluid stream. This preliminary campaign of analysis is continued in the present work by extending the range of explored angles of attack. Further numerical solutions are obtained, for steady viscous flow, past a flat plate of infinite span inclined at 9° and 15° with respect to the incoming unperturbed flow velocity. Also the influence of the free-stream turbulence intensity, at the entrance of the computational domain, is investigated, in order to obtain some practical guidelines to be used for the simulation of the flow field around inclined plates and discs.

II. THE CASE STUDY

Fage and Johansen measurements [9] were performed on a flat, sharp-edged rectangular steel plate, whose main dimensions are reported in Table I.

Marco Raciti Castelli is a Research Associate at the Department of Industrial Engineering of the University of Padova, Via Venezia 1, 35131 Padova, Italy (phone: 0039-3207179239; e-mail: marco.raciticastelli@unipd.it).

Paolo Cioppa is a M.Sc. Student in Aerospace Engineering at the Department of Industrial Engineering of the University of Padova, Via Venezia 1, 35131 Padova, Italy.

E. Benini is an Associate Professor at the Department of Industrial Engineering of the University of Padova, Via Venezia 1, 35131 Padova, Italy (e-mail: ernesto.benini@unipd.it).

TABLE I
MAIN GEOMETRICAL FEATURES OF THE FLAT PLATE ADOPTED BY FAGE AND JOHANSEN (FROM: [9])

Denomination	Value [m]
l	2.1336
b	0.1511
s	0.0045

The cross-section of the plate, normal to the span, is shown in Fig.1. In order to avoid plate deflection, the frontal surface was flat and the rear one resulted slightly tapered from the centre, where the thickness reached 3% of the chord value, towards the sharp edges. The forces on the plate, inclined at various angles to the wind, were estimated for two-dimensional flow, from pressure measurements taken in the median section. The pressure distribution over the front surface was measured for an unperturbed wind speed of 15.25 m/s.
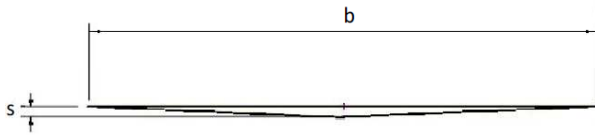

Fig. 1 Cross section of the flat plate, normal to the span

The values of the normal force coefficient k_N were estimated from the pressure coefficients along the plate, in formulas:

$$c_p = (p - p_0)/\rho V^2 \qquad (1)$$

TABLE II
MEASURED VALUES OF k_N FOR DIFFERENT PLATE INCLINATION ANGLES (FROM: [9]). THE RED RECTANGLES EVIDENCE THE REFERENCE DATA ADOPTED FOR PRESENT COMPUTATIONS

	k_N			Wind-tunnel values of $(p_m - p_0/\rho V_0^2)$	$(V_1/V_0)^2$.
α°	Wind tunnel.	Kirchhoff-Rayleigh.	Ratio of wind-tunnel k_N to theoretical k_N.		
	(A)	(B)	(C)	(D)	(E)
0	0	0	—	—	—
3	0·165	0·040	4·10	—	—
6	0·345	0·075	4·60	—	—
9	0·445	0·110	4·05	—	—
15	0·425	0·170	2·50	—	—
20	0·470	0·215	2·20	—	—
30	0·645	0·280	2·30	−0·462	1·92
40	0·785	0·335	2·35	−0·544	2·09
50	0·900	0·375	2·40	−0·615	2·23
60	0·985	0·405	2·45	−0·664	2·33
70	1·035	0·425	2·45	−0·680	2·36
80	1·060	0·435	2·45	−0·688	2·38
90	1·065	0·440	2·45	−0·690	2·38

The measured values of k_N are given in Table II (2nd column). The component of the aerodynamic force acting normally with respect to the flat plate, as evidenced in Fig. 2, can be determined by:
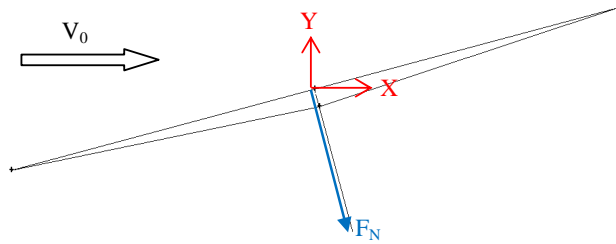
$$F_N = k_N (b \rho V_0^2) \qquad (2)$$

Fig. 2 Visualization of the component of aerodynamic force acting normally with respect to the flat plate

III. SPATIAL DOMAIN DISCRETIZATION

All the meshes adopted in the present work had common geometric features, except for the areas close to the flat plate. Inlet and outlet boundary conditions were placed respectively 12 chords upwind and 25 chords downwind with respect to the plate, allowing a full development of the wake.
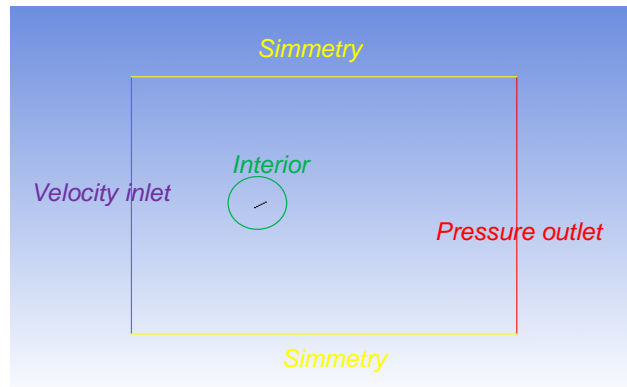

Fig. 3 Boundary conditions of the computational domain

TABLE IV
MAIN GEOMETRICAL FEATURES OF MOD0 GRID

Denomination	Value
Uniform grid spacing on the flat plate [mm]	0.7
Growth factor from the flat plate to the control circle [-]	1.1
Maximum grid dimension inside the control circle [mm]	5
Maximum grid spacing inside the computational domain [mm]	100

The discretization of the computational domain into macro-areas led to two distinct sub-grids:
- a rectangular outer zone, determining the overall calculation domain, with a circular opening centered on the flat plate;
- a circular inner zone, containing the inclined flat plate.

The circular inner zone had no physical significance: its aim was to allow a precise dimensional control of the grid elements in the area close to the flat plate by adopting a first size function, operating from the plate to the control circle itself, and a second size function, operating from the control circle to the whole computational domain.

TABLE V
MAIN GEOMETRICAL FEATURES OF MOD1 GRID

Denomination	Value
Uniform grid spacing on the flat plate [mm]	1
Growth factor from the flat plate to the control circle [-]	1.1
Maximum grid dimension inside the control circle [mm]	5
Maximum grid spacing inside the computational domain [mm]	100

TABLE VI
MAIN GEOMETRICAL FEATURES OF MOD2 GRID

Denomination	Value
Uniform grid spacing on the flat plate [mm]	1.5
Growth factor from the flat plate to the control circle [-]	1.1
Maximum grid dimension inside the control circle [mm]	5
Maximum grid spacing inside the computational domain [mm]	100

TABLE VII
MAIN GEOMETRICAL FEATURES OF MOD3 GRID

Denomination	Value
Uniform grid spacing on the flat plate [mm]	2
Growth factor from the flat plate to the control circle [-]	1.1
Maximum grid dimension inside the control circle [mm]	5
Maximum grid spacing inside the computational domain [mm]	100

TABLE VIII
MAIN GEOMETRICAL FEATURES OF MOD4 GRID

Denomination	Value
Uniform grid spacing on the flat plate [mm]	4
Growth factor from the flat plate to the control circle [-]	1.1
Maximum grid dimension inside the control circle [mm]	10
Maximum grid spacing inside the computational domain [mm]	100

Two *Symmetry* boundary conditions were adopted for the two side walls. The circumference around the circular opening, centered on the flat plate, was set as an *Interface*, thus ensuring the continuity of the flow field. Fig. 3 shows the boundary conditions of the computational domain. An unstructured mesh was chosen, in order to reduce engineering time to prepare the CFD simulations and also in order to test the prediction capability of a very simple grid. Considering their features of flexibility and adaption capability, unstructured meshes are in fact very easy to obtain, also for complex geometries, and often represent the "first attempt" to get a quick response from the CFD in engineering work.
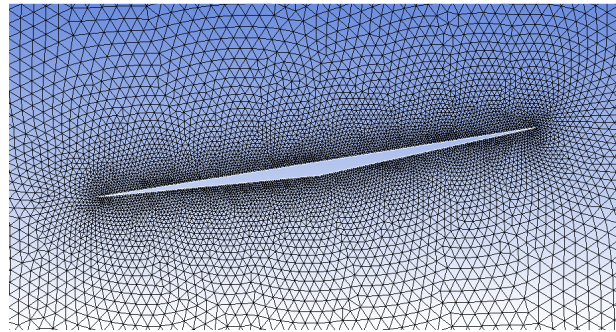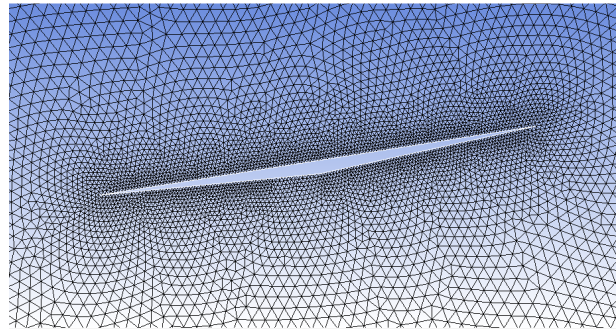
Fig. 4 Near-plate grid distribution; α = 9°, MOD0
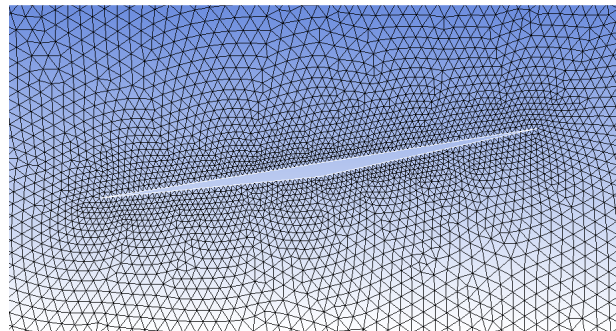
Fig. 5 Near-plate grid distribution; α = 9°, MOD1

Fig. 6 Near-plate grid distribution; α = 9°, MOD2
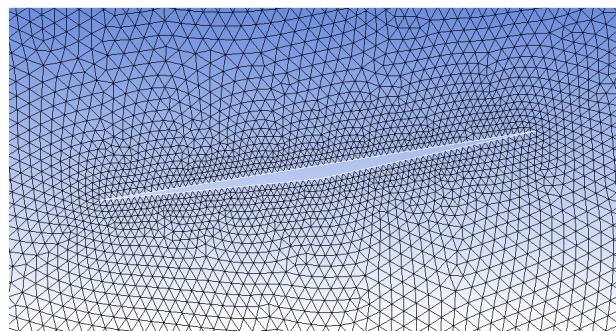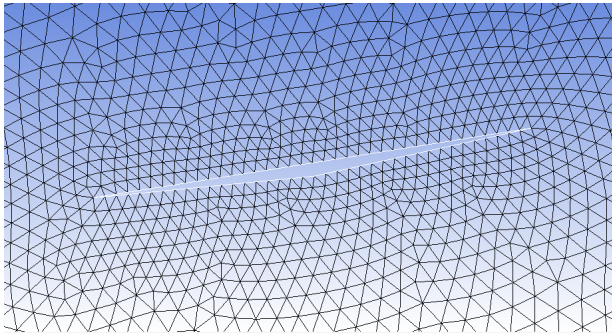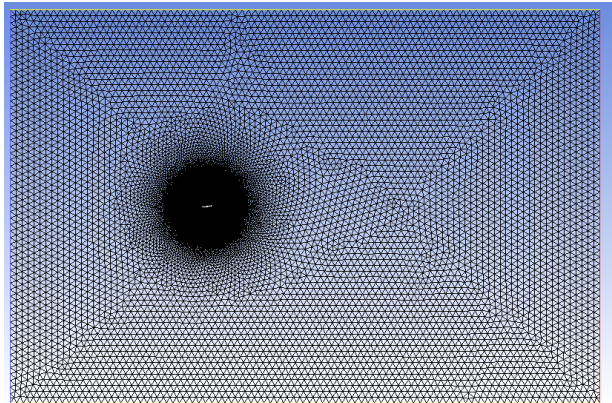
Fig. 7 Near-plate grid distribution; α = 9°, MOD3

Fig. 8 Near-plate grid distribution; α = 9°, MOD4

Fig. 9 View of the whole computational domain grid distribution; α = 9°, MOD1

In order to test the numerical code sensitivity to grid resolution, five different near-plate meshes were analyzed in the present work. Tables from IV to VIII show the main features of the adopted grid architectures, which are also reproduced in Figs. from 4 to 8, while Fig. 9 displays a view of the grid of the whole computational domain, showing also the control circle.

IV. TURBULENCE MODELS AND CONVERGENCE CRITERIA

The CFD software Ansys Fluent ® was adopted to numerically determine the surface pressure distribution on the inclined flat plate. Through its integration along the upwind and downwind faces of the flat plate, a net force vector was obtained.

Calculations were completed using the following turbulence models:

- *Standard k-ε*;
- *Realizable k-ε*, using the *Standard Wall Functions* (*SWF*) option;
- *Realizable k-ε*, using the *Non-Equilibrium Wall Functions* (*NEWF*) option;
- *NRG k-ε*.

Calculations were run until small residuals were obtained (~10^{-5}). Each simulation, performed on a 2.33 GHz clock frequency quad core CPU with Hyper-Threading, required a total computational time of about 2 hours.

V. ANALYZED RANGE OF FREE-STREAM TURBULENCE INTENSITY

The effect of percentage free-stream turbulence intensity, defined as the ratio of the root mean square of the velocity fluctuations v, to the mean free-stream velocity V, in formulas:

$$\text{FSTI} = v/V \cdot 100 \tag{3}$$

on the computed aerodynamic forces acting on the flat plate was explored through a full campaign of numerical simulations for α = 9° and *Realizable k-ε* turbulence model, using the *Standard Wall Functions* (*SWF*) option.

Table IX shows the adopted values of turbulent kinetic energy, which is related to the free-stream turbulence intensity by the formula:

$$k = 3/2 \ (V \cdot \text{FSTI})^2 \tag{4}$$

TABLE IX
VALUES OF TURBULENT KINETIC ENERGY ADOPTED FOR THE PROPOSED
NUMERICAL SIMULATIONS

k [-]	0.50	0.75	1.00	1.25	1.50

VI. RESULTS AND DISCUSSION

Figs. from 10 to 12 represent a comparison between experimentally measured (from: [9]) and numerically predicted normal force coefficients, as a function of both grid spacing and turbulence models. The resulting normal force coefficient deviations with respect to the experimental data can be determined as:

$$\Delta k_N = [(k_{N,numerical} - k_{N,experimental})/k_{N,experimental}] \cdot 100 \tag{5}$$

As can be clearly seen, the best results – based on the averaged normal force coefficient deviations with respect to the three inclination angles – were registered for *Realizable k-ε* turbulence model, adopting the *SWF* option and MOD1 grid spacing.
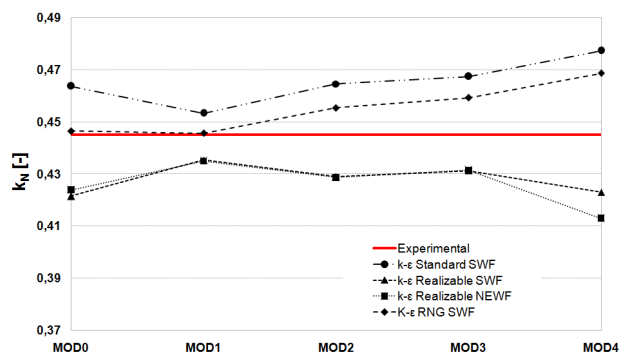

Fig. 10 Comparison between measured (from: [9]) and numerically predicted normal force coefficients, α = 9°

Table X represents the computed values of k_N, for α = 9°, MOD1 grid and *Realizable k-ε* turbulence model adopting the

SWF option, as a function of the percent free-stream turbulence intensity at the entrance of the computational domain. The numerical results need however to be interpreted, since the experimental data are affected by the uncertainty on the turbulence intensity level. In order to overcome this source of uncertainty, several values of percent free-stream turbulence intensity were investigated.
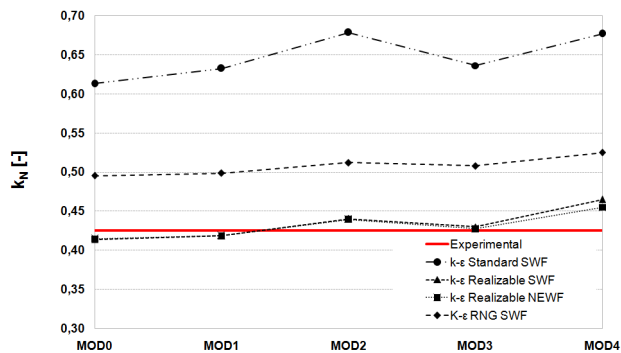

Fig. 11 Comparison between measured (from: [9]) and numerically predicted normal force coefficients, $\alpha = 15°$
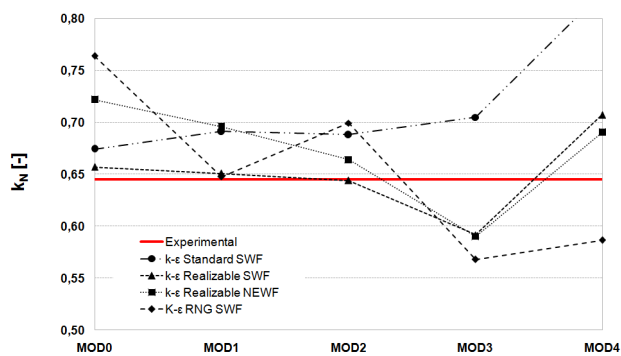

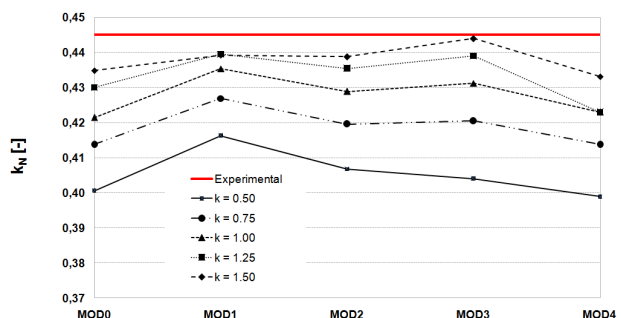Fig. 12 Comparison between measured (from: [9]) and numerically predicted normal force coefficients, $\alpha = 30°$

Fig. 13 Effect of turbulent kinetic energy on the computed normal force coefficients, $\alpha = 9°$, *Realizable k-ε* turbulence model, using the *Standard Wall Functions (SWF)* option

It can be clearly seen that the computed aerodynamic forces on the inclined plate tend to grow with the increase of the percent free-stream turbulence intensity. Moreover, as already observed by Benini and Ponza [11] and by Raciti Castelli et al.

[12], the effect of free-stream turbulence intensity on computed airfoil aerodynamic characteristics is dramatically relevant, being the sensitivity of the CFD code to turbulence intensity much higher than to the wall y^+ parameter.

TABLE X
COMPUTED VALUES OF k_N [-] AS A FUNCTION OF THE PERCENT FREE-STREAM TURBULENCE INTENSITY FOR 9° ANGLE OF ATTACK

	MOD0	MOD1	MOD2	MOD3	MOD4
FSTI = 3.79%	0.401	0.416	0.407	0.404	0.399
FSTI = 4.64%	0.414	0.427	0.420	0.420	0.414
FSTI = 5.35%	0.421	0.435	0.429	0.431	0.423
FSTI = 5.99%	0.430	0.440	0.435	0.439	0.423
FSTI = 6.56%	0.435	0.439	0.439	0.444	0.433

NOMENCLATURE

b [m]	flat plate chord
c_p [-]	pressure coefficient
F_N [N]	normal force per unit length of the plate
FSTI [%]	percentage free-stream turbulence intensity
l [m]	plate length in the span-wise direction
k [-]	turbulent kinetic energy
k_N [-]	normal force coefficient
$k_{N,experimental}$ [-]	measured normal force coefficient
$k_{N,numerical}$ [-]	computed normal force coefficient
p [Pa]	static pressure
p_0 [Pa]	static pressure of the unperturbed free-stream
s [m]	plate thickness
v [m/s]	root mean square of the velocity fluctuations
V [m/s]	air velocity
Δk_N [%]	deviation of the numerically predicted normal force coefficient with respect to the experimental data
μ [Pa·s]	air dynamic viscosity (assumed $1.789 \cdot 10^{-5}$)
ρ [kg/m³]	unperturbed air density (assumed 1.225).

REFERENCES

[1] M. Breuer and N. Jovicic, "Separated flow around a flat plate at high incidence: an LES investigation", *Journal of Turbulence*, Volume 2, Issue 1, pp. 018 (2001).
[2] A. Kasniunas, T. Robertson and Z. Howe, *Hovercraft*, Rose-Hulman Institute of Technology, Terre Haute (Indiana), 2007.
[3] R. Yoshida, T. Yamamura and K. Kadota, "Propulsive Air Stream Deflecting Apparatus for Air Cushion Vehicle", *United States Patent No. 5,007,495*, Issued on Apr. 16, 1991.
[4] C. I. Cosoiu, A. Damian, R. M. Damian and M. Degeratu, "Numerical and experimental investigation of wind induced pressures on a photovoltaic solar panel", *4th IASME/WSEAS International Conference on Energy, Environment, Ecosystems and Sustainable Development (EEESD'08)*, Algrave (Portugal), June 11-13, 2008.
[5] Y. K. Suh and C. S. Liu, "Study on the flow structure around a flat plate in a stagnation flow field", *Journal of Fluid Mechanics*, 214, pp. 469-487, doi: 10.1017/S0022112090000210, 1990.

[6]   K. Taira, W. B. Dickson, T. Colonius, M. H. Dickinson and C. W. Rowley, "Unsteadiness in flow over a flat plate at angle-of-attack at low Reynolds numbers", *AIAA Paper 2007-710*, 45th AIAA Aerospace Sciences Meeting and Exhibit , January 2007.

[7]   V. V. Bakić, G. S. Zivković and M. L. Pezo, "Numerical Simulation of the Air Flow around the Arrays of Solar Collectors", *Thermal Science*, Vol. 15, No. 2 (2011), pp. 457-465.

[8]   M. Raciti Castelli, P. Cioppa, E. Benini, "Numerical Simulation of the Flow Field around a Vertical Flat Plate of Infinite Extent", World Academy of Science, Engineering and Technology, Issue 61, 2012, pp. 284-289.

[9]   A. Fage and F. C. Johansen, "On the flow of air behind an inclined flat plate of infinite span", *Brit. Aero. Res. Coun. Rep. Memo. 1104*, pp. 81-106 (1927).

[10] M. Raciti Castelli, P. Cioppa, E. Benini, "Numerical Simulation of the Flow Field around a 30° Inclined Flat Plate", *ICAMAME 2012: International Conference on Aerospace, Mechanical, Automotive and Materials Engineering*, Florence (Italy), February 28-29, 2012.

[11] E. Benini and R. Ponza, "Laminar to Turbulent Boundary Layer transition Investigation on a Supercritical Airfoil Using the γ-θ Transitional Model", *40th Fluid Dynamics Conference and Exhibit*, 28 June – 1 July 2010, Chicago, Illinois, AIAA 2010-4289.

[12] M. Raciti Castelli, F. Garbo, E. Benini, "Turbulent Boundary Layer Transition on a Naca 0012 Airfoil for Vertical-Axis Wind Turbine Applications", *Wind Engineering*, Vol. 35, No. 6, 2011, pp. 661-686.